PLANAR TRANSLATIONAL CABLE-DIRECT-DRIVEN ROBOTS

Robert L. Williams II[1]
Ohio University
Athens, Ohio

Paolo Gallina[2]
University of Trieste
Trieste, Italy

Jigar Vadia[3]
Ohio University
Athens, Ohio

Journal of Robotic Systems
Vol. 20, No. 3, pp. 107-120
2003

ABSTRACT

We present the simulated dynamics and control of a planar, translational cable-direct-driven robot (CDDR). The motivation behind this work is to improve the serious cable interference problem with existing CDDRs and to avoid configurations where negative cable tensions are required to exert general forces and moments on the environment and during dynamic motions. Generally for CDDRs the commanded rotations are more demanding than commanded translations in terms of slack cable conditions. Therefore we propose a translational CDDR whose end-effector may be fitted with a traditional serial wrist mechanism to provide rotational freedom (assuming proper design to resist the moments). Only the translational CDDR is considered in this article, including kinematics and statics modeling, statics workspace (wherein all possible Cartesian forces and moments may be exerted with only positive cable tensions), plus a dynamics model and simulated control for planar CDDRs. Here we focus only on planar CDDRs, to clearly demonstrate our dynamics and control work; we will extend this work to spatial CDDRs in the future. Examples are presented to demonstrate simulated control including feedback linearization of the 4-cable CDDR (with one degree of actuation redundancy) performing a Cartesian task. An on-line dynamic minimum torque estimation algorithm is introduced to ensure all cable tensions remain positive for all motion; otherwise slack cables can result from CDDR dynamics and control is lost.

[1] Associate Professor
[2] Associate Professor, Visiting Researcher
[3] Graduate Research Assistant

1. INTRODUCTION

Cable-direct-driven robots (CDDRs) are a type of parallel manipulator wherein the end-effector link is supported in-parallel by *n* cables with *n* tensioning motors. In addition to the well-known advantages of parallel robots relative to serial robots, CDDRs can have lower mass than other parallel robots. Several CDDRs and cable-direct-driven haptic interfaces (CDDHIs) have been studied in the past. An early CDDR is the *Robocrane*[1] developed by NIST for use in shipping ports. This device is similar to an upside-down six-degrees-of-freedom (dof) Stewart platform, with six cables instead of hydraulic-cylinder legs. In this system, gravity ensures that cable tension is maintained at all times. Another CDDR is *Charlotte*, developed by McDonnell-Douglas[2] for use on International Space Station. *Charlotte* is a rectangular box driven in-parallel by eight cables, with eight tensioning motors mounted on-board (one on each corner). Four CDDHIs have been built and tested, the *Texas 9-string*[3], the *SPIDAR*[4], the 7-cable master[5], and the 8-cable haptic interface[6]. CDDRs and CDDHIs can be made lighter, stiffer, safer, and more economical than traditional serial robots and haptic interfaces since their primary structure consists of lightweight, high load-bearing cables. On the other hand, one major disadvantage is that cables can only exert tension and cannot push on the end-effector.

All of the devices discussed above are designed with actuation redundancy, i.e. more cables than wrench-exerting degrees-of-freedom (except for the *Robocrane*[1], where cable tensioning is provided by gravity) in attempt to avoid configurations where certain wrenches require an impossible compression force in one or more cables. Despite actuation redundancy, there exist subspaces in the potential workspace where some cables can lose tension. This problem can be exacerbated by CDDR dynamics, hence the current article studies dynamics and control of planar CDDRs. Roberts et al.[7] developed an algorithm for CDDRs to predict if all cables are under tension in a given configuration while supporting the robot weight only. They also present the inverse kinematics and fault tolerance of Charlotte-type[2] CDDRs, but no dynamics modeling is presented. The current authors (first two) have developed best CDDHI design with regard to wrenches

with only positive cable tensions and with regard to avoiding cable interference[8]. It was found that cable interference dominates.

Choe et al.[9] present stiffness analysis for wire-driven robots. Wire driven robots must provide stiffness in all 6 Cartesian degrees of freedom even if motion is in a subspace of the general case. In the current article we handle this by assuming the planar end effector is supported on a plane; thus only the *x*, *y*, and rotation about *z* freedoms must provide stiffness from the cable drive systems. Kock and Schumacher[10] have implemented a parallel robot (not cable-suspended) with actuation redundancy. They use this actuation redundancy to avoid backdriving the gear boxes and also to allow torque optimization. Barette and Gosselin[11] present general velocity and force analysis for planar cable-actuated mechanisms. They introduce and determine dynamic workspace, dependent on end-effector accelerations.

Most proposed CDDRs and CDDHIs involve both translational and rotational motion of the end-effector link guided by cables. (An exception is the *SPIDAR*[4] which is a spatial 4-cable haptic interface reading translations only and providing three Cartesian forces (no moments) to the human finger.) All CDDRs and CDDHIs with translational and rotational motion suffer from the potential of cable interference and reduced statics workspaces wherein some negative cable tensions would be required, which is infeasible. The basic idea behind this article is to provide translational motion and forces by cables; the rotational motion and moments (not studied in the current article) would then be provided by a serial wrist mechanism mounted at the end-effector of the translational CDDR. Proper design is required to ensure that the translational CDDR end-effector has sufficient stiffness in all directions to resist the rotational moments. The main objective of this work is to benefit from potential advantages of CDDRs without the cable interference and negative cable tension problems.

This article describes a planar four-cable CDDR, followed by kinematics modeling, statics modeling, a method for attempting to maintain positive cable tensions, and a discussion of the statics workspace. The article then presents dynamics modeling (resulting in a nonlinear, coupled dynamics model), followed by

Cartesian trajectory control simulation employing Cartesian PD control and feedback linearization for planar CDDRs with one degree of actuation redundancy. An on-line dynamic minimum torque estimation algorithm is developed to avoid slack cables due to CDDR dynamics. Examples are then presented for simulated control of the planar translational 4-cable CDDR.

2. CABLE-DIRECT-DRIVEN ROBOTS (CDDRs)

2.1 Four-Cable CDDR Model

In this article a CDDR consists of a single end-effector rigid body supported in parallel by n cables controlled by n tensioning actuators. Figure 1 shows the planar 4-cable CDDR kinematics diagram. We are introducing the concept of hybrid CDDRs, where the translational freedoms are provided by the n=4 cables and the rotational freedoms can be provided by a serial wrist mechanism mounted to the translational CDDR end-effector. We are considering only the translational portion of the problem here; we will attempt to keep zero orientation by control ($\phi = 0$ for all motion; ϕ, not shown in Fig. 1, is the angle between the horizontal end-effector side a and the horizontal ground link L_B). If the end-effector is supported by a base plate in the XY plane, the cross-cable configuration of Fig. 1 is sufficient in general to resist moments about the Z axis from a serial wrist mechanism consisting of a single revolute joint rotating about the Z axis, mounted to the end-effector centroid.

For 3-dof planar motions (2 translations XY and 1 rotation about Z) there must be at least three cables. Since cables can only exert tension on the end-effector, there must be more cables to avoid configurations where the robot cables can be slack and lose control. Figure 1 represents one degree of actuation redundancy, i.e. four cables to achieve the three Cartesian degrees-of-freedom $\mathbf{X} = \{x \quad y \quad \phi = 0\}^T$. This scenario represents actuation redundancy but not kinematic redundancy. That is, there is an extra motor which provides infinite choices for applying 3-dof Cartesian wrench vectors, but the moving rigid body has only three Cartesian degrees-of-freedom $\mathbf{X} = \{x \quad y \quad \phi\}^T$.

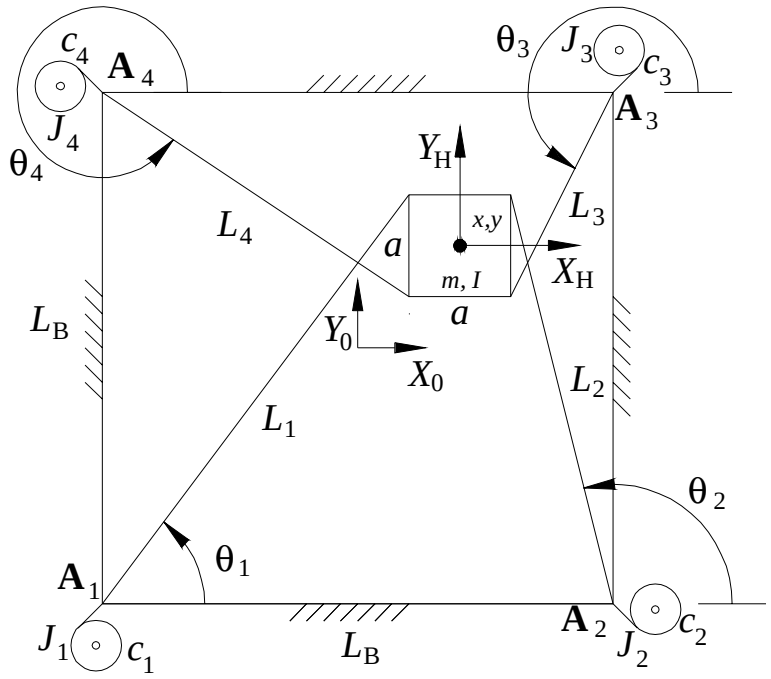

Figure 1. Planar 4-Cable CDDR Diagram

Figure 1 shows the inertially-fixed reference frame {**0**} whose origin is the centroid of the base square. The base square has sides of fixed length L_B. Each cable is passed through the ground link at the fixed points $\mathbf{A}_i = \{A_{ix} \quad A_{iy}\}^T$. The length of each cable is denoted as L_i, and the cable angles are θ_i ($i = 1,\cdots,4$). The moving end-effector frame {**H**} is also shown in Fig. 1. Note vector $\{x \quad y\}^T$ gives the position of {**H**} with respect to the {**0**} origin, expressed in {**0**} coordinates. The end-effector rigid body mass and mass moment of inertia are *m* and *I*, and the lumped motor shaft/cable pulley rotational inertias for each actuator are J_i ($i = 1,\cdots,4$). We also include viscous damping coefficients c_i ($i = 1,\cdots,4$) at each motor shaft to provide a linear model for the system friction. The cable pulley radius for each actuator is r_i ($i = 1,\cdots,4$; not shown in Fig. 1).

Theoretically the end-effector center can reach any *xy* point within the base square (reduced on the left and right sides by half the end-effector dimension, *a*/2, and increased on the top and bottom by *a*/2), if cable lengths can go to zero. A singular condition exists when the edge of the square end-effector aligns with an edge of the base square. In this case two adjacent cables align with the base plate edge; infinite force is

required in the two adjacent cables to move the end-effector normal to the aligned cables. The other two cables cannot push so motion is restricted to this reduced base square; large cable tensions will be required as this edge of motion is approached.

Cable interference is a potential problem in CDDRs. Using crossed cables as shown in Fig. 1, there will always be cable/cable contact for all motion; to avoid this problem either select low-friction cable materials to allow cables to slide freely over each other, or mount the cables in different planes, if the base plate sufficiently supports the end-effector. In the design of Fig. 1, cable/end-effector interference is non-existent in the useful motion range if we succeed in maintaining orientation $\phi = 0$ by control. In the singularities at the edge of the useful motion range, two cables will have just touched the square end-effector side, even with $\phi = 0$. The potential exists for interference between cables and workspace items and/or humans, but this problem can be minimized by design in the case of planar CDDRs.

2.2 CDDR Kinematics Modeling

Kinematics modeling is concerned with relating the active joint variables and rates to the Cartesian pose and rate variables of the end-effector. The intermediate, passive cable angles and rates are also involved. Assuming all cables always remain in tension, CDDR kinematics is similar to in-parallel-actuated robot kinematics (e.g.[13,14]); however, with CDDRs the joint space is overconstrained with respect to the Cartesian space.

The inverse pose kinematics solution is straight-forward (given the pose, calculate the cable lengths) since the end-effector configuration is completely given and the required cable lengths are simply the Euclidean norms of the cable vectors connecting each base point with the appropriate end-effector corner. The forward pose kinematics problem requires the solution of overconstrained coupled nonlinear equations and is more difficult. A Newton-Raphson numerical solution has been employed, where the overconstrained Moore-Penrose pseudoinverse is used in the iteration. The CDDR inverse velocity Jacobian matrix is closely

related to the Newton-Raphson Jacobian matrix and the statics Jacobian matrix. These kinematics solutions are presented in[6] and will not be repeated here.

3. CDDR STATICS MODELING

In this article, the workspace wherein all cables are under positive tension while exerting all possible Cartesian wrenches is called the statics workspace. Statics modeling and attempting to maintain positive cable tension for all wrenches are presented in this section. We use a simple method to determine the extent of the statics workspace, i.e. the workspace wherein all possible end-effector wrenches can be resisted with only positive cable tensions.

3.1 Statics Modeling

This section presents statics modeling for planar CDDRs. For static equilibrium the sum of external forces and moments exerted on the end-effector by the cables must equal the resultant external wrench exerted on the environment (or, the wrench exerted by a serial wrist mechanism acting on the environment must react on the CDDR end-effector). Figure 2 shows the statics free-body diagram for the planar 4-cable CDDR.

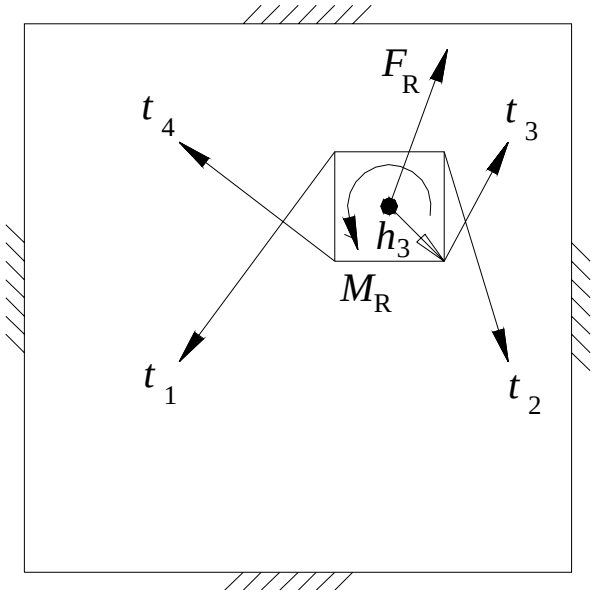

Figure 2. Planar 4-Cable CDDR Statics Diagram

The statics equations are:

$$\sum_{i=1}^{4}\mathbf{t}_i = -\sum_{i=1}^{4} t_i\hat{\mathbf{L}}_i = \mathbf{F}_R \qquad\qquad \sum_{i=1}^{4}\mathbf{m}_i = \sum_{i=1}^{4}\left({}^{0}_{H}\mathbf{R}\mathbf{h}_i\right)\times\mathbf{t}_i = \mathbf{M}_R \tag{1}$$

In this article gravity is ignored because it is assumed to be perpendicular to the CDDR plane; we assume the end-effector is supported on a base plate with negligible friction. The definition of frames {**0**} and {**H**} are given in Fig. 1. In (1), t_i is the cable tension applied to the i^{th} cable (in the negative cable length unit direction $\hat{\mathbf{L}}_i$ because $\mathbf{t}_i$ must be in tension); ${}^{0}_{H}\mathbf{R}$ is the orthonormal rotation matrix relating the orientation of {**H**} to {**0**} (nominally, ${}^{0}_{H}\mathbf{R} = \mathbf{I}_3$ since we are controlling for zero orientation, ϕ=0); $\mathbf{h}_i$ is the position vector from the origin of {**H**} to the i^{th} cable connection, expressed in {**H**} coordinates (only $\mathbf{h}_3$ is shown in Fig. 2); and $\mathbf{F}_R$ and $\mathbf{M}_R$ are the resultant vector force and moment (taken together, wrench) exerted on the environment. Substituting the above terms into (1) yields:

$$\mathbf{S}\mathbf{T} = \mathbf{W}_R \tag{2}$$

$\mathbf{T} = \begin{Bmatrix} t_1 & t_2 & t_3 & t_4 \end{Bmatrix}^T$ is the vector of scalar cable forces, $\mathbf{W}_R = \begin{Bmatrix} \mathbf{F}_R & \mathbf{M}_R \end{Bmatrix}^T = \begin{Bmatrix} F_{Rx} & F_{Ry} & M_{Rz} \end{Bmatrix}^T$ is the resultant external end-effector wrench vector (expressed in {**0**} coordinates but felt at the origin of {**H**}), and the 3*x*4 Statics Jacobian matrix $\mathbf{S}$ (expressed in {**0**} coordinates) is:

$$\mathbf{S} = \begin{bmatrix} -\hat{\mathbf{L}}_1 & -\hat{\mathbf{L}}_2 & -\hat{\mathbf{L}}_3 & -\hat{\mathbf{L}}_4 \\ \hat{\mathbf{L}}_1\times{}^{0}_{H}\mathbf{R}\mathbf{h}_1 & \hat{\mathbf{L}}_2\times{}^{0}_{H}\mathbf{R}\mathbf{h}_2 & \hat{\mathbf{L}}_3\times{}^{0}_{H}\mathbf{R}\mathbf{h}_3 & \hat{\mathbf{L}}_4\times{}^{0}_{H}\mathbf{R}\mathbf{h}_4 \end{bmatrix} \tag{3}$$

The specific (3) expressions for the Fig. 1 CDDR are:

$$\mathbf{S} = \begin{bmatrix} -c\theta_1 & -c\theta_2 & -c\theta_3 & -c\theta_4 \\ -s\theta_1 & -s\theta_2 & -s\theta_3 & -s\theta_4 \\ c\theta_1 h_{1y} - s\theta_1 h_{1x} & c\theta_2 h_{2y} - s\theta_2 h_{2x} & c\theta_3 h_{3y} - s\theta_3 h_{3x} & c\theta_4 h_{4y} - s\theta_4 h_{4x} \end{bmatrix} \tag{4}$$

where $\mathbf{h}_i = \begin{Bmatrix} h_{ix} & h_{iy} \end{Bmatrix}^T$, $c\theta_i = \cos\theta_i$, and $s\theta_i = \sin\theta_i$. Equation (4) assumes that the orientation is $\phi = 0$ for all pseudostatic motion; otherwise each third row term of (4) is: $c\theta_i\left(h_{ix}s\phi + h_{iy}c\phi\right) - s\theta_i\left(h_{ix}c\phi - h_{iy}s\phi\right)$. This assumption is fine for pseudostatic motion, but in the dynamics modeling section we will use the general

form where $\phi \neq 0$ since dynamics can cause small errors in ϕ despite control attempts to make $\phi = 0$. The statics equations (2) can be inverted in an attempt to resist general (in this article, planar) Cartesian wrenches while maintaining positive cable tension. This work is presented in the next subsection.

3.2 Maintaining Positive Cable Tension

For CDDRs with actuation redundancy, (2) is underconstrained which means that there are infinite solutions to the cable tension vector $\mathbf{T}$ to exert the required Cartesian wrench $\mathbf{W}_R$. To invert (2) (solving the required cable tensions $\mathbf{T}$ given wrench $\mathbf{W}_R$) we adapt the well-known particular and homogeneous solution from rate control of kinematically-redundant serial manipulators:

$$\mathbf{T} = \mathbf{S}^{+}\mathbf{W}_R + \left(\mathbf{I}_n - \mathbf{S}^{+}\mathbf{S}\right)\mathbf{z} \tag{5}$$

where $\mathbf{I}_n$ is the *n*x*n* identity matrix, $\mathbf{z}$ is an arbitrary *n*-vector, and $\mathbf{S}^{+} = \mathbf{S}^T\left(\mathbf{S}\mathbf{S}^T\right)^{-1}$ is the *n*x3 underconstrained Moore-Penrose pseudoinverse of **S**. The first term of (5) is the particular solution to achieve the desired wrench, and the second term is the homogeneous solution that projects $\mathbf{z}$ into the null space of **S**.

For CDDRs with one degree of actuation redundancy (the case in this article), the positive cable tension method of Shen et al.[12] is adapted to determine the extent of the statics workspace. For actuation redundancy of degree one, an equivalent expression for (5) is:

$$\mathbf{T} = \begin{Bmatrix} t_{P1} \\ t_{P2} \\ t_{P3} \\ t_{P4} \end{Bmatrix} + \alpha \begin{Bmatrix} n_1 \\ n_2 \\ n_3 \\ n_4 \end{Bmatrix} \tag{6}$$

where the particular solution $\mathbf{S}^{+}\mathbf{W}_R$ is the first term in (6) and the homogeneous solution is expressed as the kernel vector $\mathbf{N}$ of $\mathbf{S}$ ($\mathbf{N} = \{n_1 \quad n_2 \quad n_3 \quad n_4\}^T$) multiplied by arbitrary scalar α.

The method we adapt from Shen et al.[12] to determine if a given point lies within the statics workspace for a given CDDR is simple. To ensure positive tensions t_i on all cables $i = 1,\cdots,4$, *for all possible exerted forces and moments*, it is necessary and sufficient that all kernel vector components (n_i, $i = 1,\cdots,4$) have the same sign. That is, for a given point to lie within the statics workspace, all $n_i > 0$ OR all $n_i < 0$ ($i = 1,\cdots,4$). If one of these two conditions is satisfied, regardless of the particular solution, we can find a scalar α in (6) which guarantees that all cable tensions **T** are positive by adding (or subtracting) enough homogeneous solution. Note a strict inequality is required; if one or more $n_i = 0$, the CDDR configuration in question does not lie within the statics workspace. This method is simple but powerful since we needn't consider specific wrenches: it works for *all possible wrenches*. It should also be noted that while we demonstrate this method for the planar 4-cable CDDR, it is applicable to any planar and spatial CDDR with one degree of actuation redundancy.

A symbolic expression for the kernel vector (null space basis) of the 4-cable CDDR (with $\phi = 0$) is:

$$\mathbf{N} = \begin{Bmatrix} n_1 \\ n_2 \\ n_3 \\ n_4 \end{Bmatrix} = \begin{Bmatrix} \cos(\theta_2 - \theta_3 - \theta_4) - \cos(\theta_2 - \theta_3 + \theta_4) + \sin(\theta_2 - \theta_3 + \theta_4) - \sin(\theta_2 + \theta_3 - \theta_4) \\ \cos(\theta_1 + \theta_3 - \theta_4) - \cos(\theta_1 - \theta_3 - \theta_4) + \sin(\theta_1 + \theta_3 - \theta_4) - \sin(\theta_1 - \theta_3 + \theta_4) \\ \cos(\theta_1 - \theta_2 - \theta_4) - \cos(\theta_1 + \theta_2 - \theta_4) + \sin(\theta_1 - \theta_2 - \theta_4) + \sin(\theta_1 - \theta_2 + \theta_4) \\ \cos(\theta_1 + \theta_2 - \theta_3) - \cos(\theta_1 - \theta_2 + \theta_3) - \sin(\theta_1 - \theta_2 - \theta_3) - \sin(\theta_1 - \theta_2 + \theta_3) \end{Bmatrix} \tag{7}$$

Now, the allowable cable angle ranges are $0 < \theta_1 < 90^\circ$, $90^\circ < \theta_2 < 180^\circ$, $180^\circ < \theta_3 < 270^\circ$, and $270^\circ < \theta_4 < 360^\circ$. For these allowable angle ranges, by careful consideration of sums/differences of the three distinct angle combinations in each row of (7) we have proven (not shown for lack of space) that the sign of ALL n_i components is always the same, $i = 1,\cdots,4$. Therefore, *the entire allowable kinematic workspace of the base square is also the statics workspace*! Now, when the edge of the end-effector square is aligned with an edge of the base square, two components $n_i = 0$ and thus the allowable statics workspace is the base square, reduced by *a*/2 (half the end-effector side) on the left and right and increased by *a*/2 on the top and bottom (with regard to Fig. 1). This edge singularity condition was discussed earlier in Section 2.1.

At all points outside of the base square, all components of the kernel vector **N** do not have the same sign so outside the useful region of the base square is also outside of the statics workspace. This statics workspace discussion holds only for $\phi = 0$, the nominal case of the planar translational CDDR. In previous work, it was discovered that the statics workspace is extremely limited when considering general ϕ rotations[8].

For real-time pseudostatic control of a planar CDDR with one degree of actuation redundancy, the cable tensions for control are calculated by (6) and (7), choosing α so that one component of **T** is zero (or, a small positive tension value) and the remaining terms are positive.

Since the pseudostatic condition is a limiting subset of the general dynamics case, especially for high velocities and accelerations, we now move on to dynamics modeling.

4. CDDR DYNAMICS MODELING

This section presents dynamics modeling for planar CDDRs. The 4-cable planar translational CDDR is shown in Fig. 1. Dynamics modeling is required for improved control (compared to using kinematics and statics modeling only) when CDDRs are to provide high velocities and accelerations in translational motion. Dynamics modeling is concerned with relating the Cartesian translational motion of the moving CDDR end-effector to the required active joint torques. Due to the cable actuation, CDDR dynamics modeling is not very similar to in-parallel-actuated robot dynamics modeling (e.g.[13,14]). Another complicating factor is that the joint space is overconstrained with respect to the Cartesian space due to redundant actuation. Also, though we are presenting a translational CDDR, we include the rotational motion in the dynamics equations so we can evaluate how effective our $\phi = 0$ control is in simulation.

For the dynamics model derived in this section we assume that the CDDR cables are massless and perfectly stiff so we do not consider their inertias or spring stiffnesses. We further ignore the Coulomb friction and instead model linear viscous friction to account for the frictional losses. Despite these simplifications, the resulting model is coupled and nonlinear. We now present the Cartesian, actuator, and overall system dynamics models.

4.1 Cartesian Dynamics Model

The 3-*dof* Cartesian dynamic model for the planar CDDR end-effector is given by $\mathbf{M}\ddot{\mathbf{X}} = \mathbf{W}_R$:

$$\begin{bmatrix} m & 0 & 0 \\ 0 & m & 0 \\ 0 & 0 & I \end{bmatrix} \begin{Bmatrix} \ddot{x} \\ \ddot{y} \\ \ddot{\phi} \end{Bmatrix} = \begin{Bmatrix} F_{Rx} \\ F_{Ry} \\ M_{Rz} \end{Bmatrix} \tag{8}$$

where $\mathbf{M}$ is the Cartesian inertia matrix (m is the end-effector mass and I is the end-effector mass moment of inertia about the z axis through the center of mass), $\ddot{\mathbf{X}} = \{\ddot{x} \quad \ddot{y} \quad \ddot{\phi}\}^T$ is the end-effector acceleration (acceleration of the {**H**} frame with respect to the inertial frame {**0**}, expressed in {**0**} coordinates), and

$\mathbf{W}_R = \{F_{Rx} \quad F_{Ry} \quad M_{Rz}\}^T$ is the force and moment (about the center of mass) resultant of all *n* cable tensions acting on the end-effector; $\mathbf{F}_R = \{F_{Rx} \quad F_{Ry}\}^T = -\sum_{i=1}^{4} t_i \hat{\mathbf{L}}_i$ and $\mathbf{M}_R = M_{Rz}\hat{k} = \sum_{i=1}^{4} \left({}^0_H\mathbf{R}\mathbf{h}_i\right) \times \mathbf{t}_i$.

4.2 Actuator Dynamics Model

We also take into consideration the dynamic behavior of the lumped motor shaft/cable pulley; the free-body diagram for the i^{th} motor shaft/cable pulley subsystem is shown in Fig. 3.

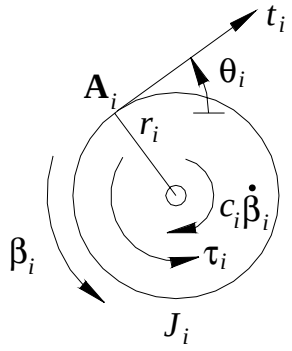

Figure 3. Free-Body Diagram for the i^{th} Pulley/Shaft

The combined motor shaft/cable pulley dynamics equations are expressed by the relationship:

$$\mathbf{J}\ddot{\boldsymbol{\beta}} + \mathbf{C}\dot{\boldsymbol{\beta}} = \boldsymbol{\tau} - r\mathbf{T} \tag{9}$$

where: $\mathbf{J} = \begin{bmatrix} J_1 & & 0 \\ & \ddots & \\ 0 & & J_n \end{bmatrix}$ and $\mathbf{C} = \begin{bmatrix} c_1 & & 0 \\ & \ddots & \\ 0 & & c_n \end{bmatrix}$

are diagonal matrices with rotational inertia and rotational viscous damping coefficients on the diagonal, all cable pulley radii (r_i in Fig. 3) are identical ($r_i = r$; $i = 1, \cdots, n$), $\boldsymbol{\tau} \in R^n$ is the vector of torques exerted by the motors, $\mathbf{T} \in R^n$ is the vector of cable tensions t_i, and $\boldsymbol{\beta} \in R^n$ is the vector of pulley angles. Since the cables can only exert positive tensions (they cannot push), to express the cable tensions as a function of the motor torques and angular motion from (9), we obtain:

$$\mathbf{T} = pos\left(\frac{1}{r}\left(\boldsymbol{\tau} - \mathbf{J}\ddot{\boldsymbol{\beta}} - \mathbf{C}\dot{\boldsymbol{\beta}}\right)\right) \tag{10}$$

where the symbol *pos*() means we take the value of each vector component that is positive and we set to zero those components that were originally negative. Let us suppose that the torque on each motor is large enough to make all cables remain in tension at all times. Under this assumption:

$$\mathbf{T} = \frac{1}{r}\left(\boldsymbol{\tau} - \mathbf{J}\ddot{\boldsymbol{\beta}} - \mathbf{C}\dot{\boldsymbol{\beta}}\right) \tag{11}$$

4.3 System Dynamics Model

We now derive the overall system dynamics model by combining the Cartesian and actuator dynamics equations of motion. The statics relationship $\mathbf{W}_R = \mathbf{ST}$ between forces on the end-effector and cable tensions was derived in Section 3.1, where the 3x*n* (*n*=4) statics Jacobian matrix **S** is given in (4). However, as mentioned in Section 3.1, here we cannot apply the pseudostatic assumption that ϕ = 0 for all motion and hence the third row of (4) must be replaced with the terms: $c\theta_i\left(h_{ix}s\phi + h_{iy}c\phi\right) - s\theta_i\left(h_{ix}c\phi - h_{iy}s\phi\right);\ i = 1,\cdots,4$, one for each column of the statics Jacobian matrix.

We now need an inverse kinematics mapping relating the pulley angles β_i ($i = 1,\cdots,n$) expressed as functions of the end-effector position and orientation $\mathbf{X} = \{x \quad y \quad \phi\}^T$. Let us define all β_i to be zero when the end-effector centroid is located at the origin of frame {**0**}, with zero orientation (ϕ = 0). From this configuration, a right-handed positive angle β_i on one pulley will cause a negative change ΔL_i in cable length *i*: $\beta_i r = -\Delta L_i$. The change in cable length *i* is $\Delta L_i = L_i - L_{0i}$ where L_i is the general length for cable *i* from the inverse pose solution and L_{0i} is the initial length for cable *i*:

$$L_i = \sqrt{\left(x - A_{ix} + h_{ix}c\phi - h_{iy}s\phi\right)^2 + \left(y - A_{iy} + h_{ix}s\phi + h_{iy}c\phi\right)^2} \qquad L_{0i} = \sqrt{\left(h_{ix} - A_{ix}\right)^2 + \left(h_{iy} - A_{iy}\right)^2} \tag{12}$$

$$\boldsymbol{\beta} = \begin{Bmatrix} \beta_1(\mathbf{X}) \\ \vdots \\ \beta_n(\mathbf{X}) \end{Bmatrix} = \frac{1}{r}\begin{Bmatrix} L_{01} - L_1 \\ \vdots \\ L_{0n} - L_n \end{Bmatrix} \tag{13}$$

Successive time derivatives of (13) yield:

$$\dot{\boldsymbol{\beta}} = \frac{\partial \boldsymbol{\beta}}{\partial \mathbf{X}} \dot{\mathbf{X}}$$
$$\ddot{\boldsymbol{\beta}} = \frac{d}{dt}\left(\frac{\partial \boldsymbol{\beta}}{\partial \mathbf{X}}\right)\dot{\mathbf{X}} + \frac{\partial \boldsymbol{\beta}}{\partial \mathbf{X}} \ddot{\mathbf{X}} \tag{14}$$

where $\frac{\partial \boldsymbol{\beta}}{\partial \mathbf{X}}$ may easily be derived; it is a function of the Cartesian pose kinematics terms. By substituting (14) into (11) we obtain:

$$\mathbf{T} = \frac{1}{r}\left(\boldsymbol{\tau} - \mathbf{J}\left(\frac{d}{dt}\left(\frac{\partial \boldsymbol{\beta}}{\partial \mathbf{X}}\right)\dot{\mathbf{X}} + \frac{\partial \boldsymbol{\beta}}{\partial \mathbf{X}} \ddot{\mathbf{X}}\right) - \mathbf{C}\frac{\partial \boldsymbol{\beta}}{\partial \mathbf{X}} \dot{\mathbf{X}}\right) \tag{15}$$

Finally, by combining (8), $\mathbf{W}_R = \mathbf{ST}$, and (15), we obtain the overall dynamics equations of motion, expressed in a standard Cartesian form for robotic systems[15]:

$$\mathbf{M}_{eq}(\mathbf{X})\ddot{\mathbf{X}} + \mathbf{N}(\mathbf{X}, \dot{\mathbf{X}}) = \mathbf{S}(\mathbf{X})\boldsymbol{\tau} \tag{16}$$

where the equivalent inertia matrix $\mathbf{M}_{eq}(\mathbf{X})$ and nonlinear terms $\mathbf{N}(\mathbf{X}, \dot{\mathbf{X}})$ are:

$$\mathbf{M}_{eq}(\mathbf{X}) = r\mathbf{M} + \mathbf{S}(\mathbf{X})\mathbf{J}\frac{\partial \boldsymbol{\beta}}{\partial \mathbf{X}} \tag{16a}$$

$$\mathbf{N}(\mathbf{X}, \dot{\mathbf{X}}) = \mathbf{S}(\mathbf{X})\left(\mathbf{J}\frac{d}{dt}\left(\frac{\partial \boldsymbol{\beta}}{\partial \mathbf{X}}\right) + \mathbf{C}\frac{\partial \boldsymbol{\beta}}{\partial \mathbf{X}}\right)\dot{\mathbf{X}} \tag{16b}$$

Note the statics Jacobian matrix $\mathbf{S} = \mathbf{S}(\mathbf{X})$ from (4) is a function of Cartesian pose $\mathbf{X} = \{x \quad y \quad \phi\}^T$ through the cable angles $\theta_i = \tan^{-1}\left(\frac{y - A_{iy} + h_{ix}s\phi + h_{iy}c\phi}{x - A_{ix} + h_{ix}c\phi - h_{iy}s\phi}\right)$ (see Fig. 1).

5. CDDR CONTROLS SIMULATION

This section presents our CDDR control architecture and control law development, followed by the method for resolving the actuation redundancy, including an algorithm for on-line estimation of minimum actuator torques in order to maintain cable tension despite CDDR dynamics.

5.1 Control Law and Architecture

This sub-section presents our control architecture and control law development for planar CDDRs based on the overall system Cartesian dynamics equations of motion (16). The input to the plant is the vector of actuator torques $\boldsymbol{\tau}$. Each component of $\boldsymbol{\tau}$ has to be positive or zero at the minimum (in practice, a small positive value). In order to facilitate this problem, let us introduce a virtual generalized Cartesian wrench input $\mathbf{W}_V$ (units *N, N, Nm*):

$$\mathbf{W}_V = \mathbf{S}(\mathbf{X})\boldsymbol{\tau} \tag{17}$$

Since the statics Jacobian matrix $\mathbf{S}(\mathbf{X})$ has dimension 3x*n*, this virtual generalized wrench input $\mathbf{W}_V$ has the dimension of the Cartesian space, 3 in this article (though we are presenting a planar translational CDDR we also need to attempt to control $\phi = 0$ for all motion). The components of $\mathbf{W}_V$ are not restricted to be positive. If we can develop a control law for the virtual Cartesian wrench input $\mathbf{W}_V$, it is always possible to find a real controls torque input vector $\boldsymbol{\tau}$ with all positive components that satisfies (17), if the CDDR pose is within the statics workspace. In Section 3.2 we found that the base square is the statics workspace for our planar translational CDDR, reduced by half the end-effector side, *a*/2, on the left and right and increased by *a*/2 on the top and bottom (see Fig. 1). Therefore, for control law development, we can consider the new dynamics equation:

$$\mathbf{M}_{eq}(\mathbf{X})\ddot{\mathbf{X}} + \mathbf{N}(\mathbf{X}, \dot{\mathbf{X}}) = \mathbf{W}_V \tag{18}$$

We cancel the effects of the nonlinear dynamics terms $\mathbf{N}(\mathbf{X}, \dot{\mathbf{X}})$ and account for the inertial terms by using the well-known computed-torque (or feedback linearization) technique[15]. We then implement a

Cartesian PD controller to reduce the tracking error $\mathbf{e} = \mathbf{X}_R - \mathbf{X}$. The commanded (reference) Cartesian pose is $\mathbf{X}_R = \{x_R \quad y_R \quad \phi_R = 0\}^T$. The computed-torque control law for the virtual Cartesian wrench input $\mathbf{W}_V$ is:

$$\mathbf{W}_V = \mathbf{M}_{eq}(\mathbf{X}_R)\left(\ddot{\mathbf{X}}_R + \mathbf{K}_P\mathbf{e} + \mathbf{K}_D\dot{\mathbf{e}}\right) + \mathbf{N}\left(\mathbf{X}_R, \dot{\mathbf{X}}_R\right) \tag{19}$$

Note we use the reference Cartesian values $\mathbf{X}_R$ in (19). Alternatively, we could use the actual feedback values from actuator encoder sensors and forward pose kinematics. Due to this uncertainty, plus sensor noise problems, plus the problem of digitally twice differentiating the sensor feedback $\mathbf{X}$, we choose $\mathbf{X}_R$ instead.

The controller architecture (shown in the block diagram of Fig. 4) is made up of three different parts: the Cartesian PD controller, the computed-torque terms, and the virtual-Cartesian-wrench-input-to-real-actuator-torque calculation, with dynamic minimum torque estimation to ensure cable tension is maintained at all times despite the CDDR dynamics. In this article the PD controller gains are determined via pole placement for the resulting effective unit inertia plant, specifying desired settling time and percent overshoot for a unit step input. The matrix gains $\mathbf{K}_P, \mathbf{K}_D$ are 3x3 diagonal matrices, which means that the PD control is accomplished independently for the *x*, *y*, and ϕ motions, even though the dynamics model is coupled. We specify the same settling time and percent overshoot for all Cartesian motions (see Section 6). The inertial terms $\mathbf{M}_{eq}(\mathbf{X}_R)\ddot{\mathbf{X}}_R$ are composed of the overall pose-dependent Cartesian inertia matrix $\mathbf{M}_{eq}(\mathbf{X}_R)$ (16a) and the reference Cartesian acceleration components $\ddot{\mathbf{X}}_R$; the nonlinear terms are $\mathbf{N}\left(\mathbf{X}_R, \dot{\mathbf{X}}_R\right)$, given in (16b). The virtual-to-real calculation has the problem to invert non-square matrix **S**(**X**), such that only positive actuator torques result given the virtual Cartesian wrench input $\mathbf{W}_V$. This problem is solved in Section 3.2 for CDDRs assuming the pseudostatic condition; this is adapted in Section 5.2 below for CDDR dynamics.

We do not generally have access directly to Cartesian pose **X** feedback via sensors. Instead, we must calculate this feedback using the encoder feedback for each cable pulley angle β_i to determine the cable lengths L_i; these lengths are then used as the inputs to the forward pose kinematics solution to calculate Cartesian pose **X** for feedback in the control architecture. This feedback scheme will work well only if sufficient tension is maintained on all cables at all times.

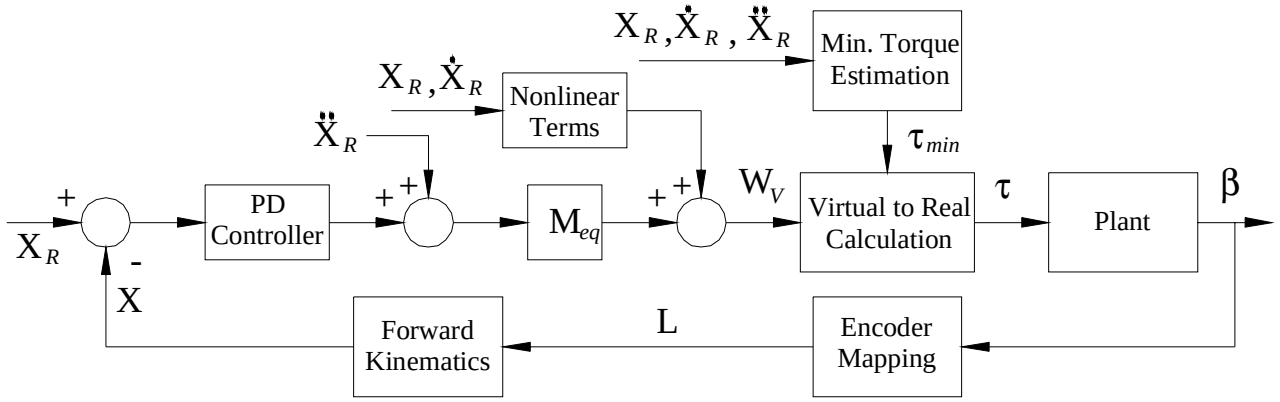

Figure 4. Controller Architecture for Planar CDDRs

5.2 Calculation of Optimal Actuator Torques

This sub-section presents a method for determining the optimal actuator torques for the controller architecture of Fig. 4. This sub-section presents the "Virtual-to-Real Calculation" block of Fig. 4. Also presented is an algorithm for on-line estimation of minimum actuator torques required to maintain positive cable tensions despite the CDDR dynamics; this is the "Min. Torque Estimation" block in Fig. 4.

The Jacobian matrix relationship between torques and virtual generalized Cartesian wrenches is underconstrained for CDDRs, given by (17), $\mathbf{W}_V = \mathbf{S}(\mathbf{X})\boldsymbol{\tau}$. For control we need to calculate the real actuator torques $\boldsymbol{\tau}$ given the virtual Cartesian control wrenches $\mathbf{W}_V$. For actuation redundancy of degree one, we can adapt the pseudostatics solution of Section 3.2 (to this method we must add the on-line, dynamic minimum torque estimation algorithm, developed below in the current sub-section). The difference from (6) is that we can no longer make the pseudostatics assumption $\tau_i = rt_i$ (τ_i is the i^{th} actuator torque, r is the

cable pulley radius, and t_i is the i^{th} cable tension). Due to dynamics this assumption no longer holds; we must calculate the required actuator torques for control while attempting to maintain positive cable tensions dynamically. The solution of the underconstrained system $\mathbf{W}_V = \mathbf{S}(\mathbf{X})\boldsymbol{\tau}$ is similar to (6), given in (20).

$$\boldsymbol{\tau}_{\text{opt}} = \begin{Bmatrix} \tau_{P1} \\ \tau_{P2} \\ \tau_{P3} \\ \tau_{P4} \end{Bmatrix} + \alpha \begin{Bmatrix} n_1 \\ n_2 \\ n_3 \\ n_4 \end{Bmatrix} > \boldsymbol{\tau}_{\min} \begin{Bmatrix} 1 \\ 1 \\ 1 \\ 1 \end{Bmatrix} \tag{20}$$

The particular solution $\mathbf{S}^{+}\mathbf{W}_V$ is the first term in (20) and the homogeneous solution is expressed as the kernel vector of $\mathbf{S}$ ($\mathbf{N} = \{n_1 \quad n_2 \quad n_3 \quad n_4\}^T$) multiplied by arbitrary scalar α. The goal of torque calculation consists in finding an optimal solution $\boldsymbol{\tau}_{\text{opt}}$ with the following features: 1) We start with the particular solution wherein the Euclidean norm of $\boldsymbol{\tau}$ is minimized. 2) We use the homogeneous solution to ensure that each component of $\boldsymbol{\tau}_{\text{opt}}$ must be greater than or equal to a specified minimum torque $\boldsymbol{\tau}_{\min}$. We must calculate α at each control cycle to ensure, in the worst component case, that this minimum positive torque is satisfied for all four actuators. This is an easy calculation for actuation redundancy of degree one; at each control cycle it is not necessarily the most negative particular torque component that dominates, but the combination of particular torque and kernel vector component that determines the dominant α. For each particular torque component that is negative, calculate $\alpha_i = (\boldsymbol{\tau}_{\min} - \boldsymbol{\tau}_{Pi})/n_i$; then select the largest magnitude of these to be the α at each control cycle. Further, α must be positive if all n_i are positive and α must be negative if all n_i are negative. This single α value of course must be then used for all four components in (20). Since the entire useful CDDR workspace is equal to the statics workspace, this α can always be found for all possible motions (i.e. the signs of n_i are always the same for all four components).

If we don't consider dynamic effects, the tension in each cable turns out to be greater than $r\boldsymbol{\tau}_{\min}$. Under this pseudostatic condition, if $\boldsymbol{\tau}_{\min}$ is set sufficiently high, the cables will never go slack.

Unfortunately, when high speed is employed, because of dynamic effects, one or more cable can become slack despite a positive $\boldsymbol{\tau}_{\min}$. In this dynamic case the minimum value for $\boldsymbol{\tau}_{\min}$ must be estimated on-line for each cable in real-time. The on-line cable tension estimation algorithm comes from forcing each tension component to be positive at all times in the dynamics model (15):

$$\{\mathbf{T}\}_i = \left\{ \frac{1}{r}\left(\tau - \mathbf{J}\left(\frac{d}{dt}\left(\frac{\partial \beta}{\partial \mathbf{X}} \right)\dot{\mathbf{X}} + \frac{\partial \beta}{\partial \mathbf{X}}\ddot{\mathbf{X}} \right) - \mathbf{C}\frac{\partial \beta}{\partial \mathbf{X}}\dot{\mathbf{X}} \right) \right\}_i \geq 0 \qquad i = 1, \cdots, n \qquad (21)$$

The estimated minimum torque solution for each actuator from (21) to maintain cable tension based on CDDR dynamics is:

$$\boldsymbol{\tau}_{\min} = \max\left\{ \left\{ \mathbf{J}\left(\frac{d}{dt}\left(\frac{\partial \beta}{\partial \mathbf{X}} \right)\dot{\mathbf{X}} + \frac{\partial \beta}{\partial \mathbf{X}}\ddot{\mathbf{X}} \right) + \mathbf{C}\frac{\partial \beta}{\partial \mathbf{X}}\dot{\mathbf{X}} \right\}_i, 0 \right\} \qquad i = 1, \cdots, n \qquad (22)$$

The reason for the max function in (22) is that when CDDR dynamics are taken into account, the minimum torque required to ensure the corresponding cable is in tension could be negative for one or more components. In (22) we force all torque components to be zero at the minimum. In practice and in the examples of the next section, we choose instead a small positive value.

6. EXAMPLES

This section presents dynamics and control examples for the planar 4-cable translational CDDR with one degree of actuation redundancy. These examples are intended to demonstrate the CDDR control architecture including feedback linearization and on-line dynamic torque estimation to maintain positive cable tensions despite the dynamics, plus optimal torque calculation for a CDDR with one degree of actuation redundancy. In this section, a given planar 4-cable CDDR performs a simulated task twice, the first time without and the second time with the on-line minimum torque estimation algorithm.

The planar translational 4-cable CDDR model is shown in Fig. 1. The following parameters are taken from a hardware system we have designed for future experimental work. The base square has side L_B = 0.70 *m* and the end-effector square has side a = 0.10 *m*. The simulated dynamic task is for the CDDR end-effector point $\mathbf{X} = \{x \quad y\}^T$ to trace a circle in the plane, while attempting to maintain $\phi = 0$ for all motion. The circle is centered at the base square centroid (the origin of $\{\mathbf{0}\}$) and the circle radius is r = 0.15 *m*. Figure 5 shows the simulated task to scale for the 4-cable CDDR at the starting (and ending) point.

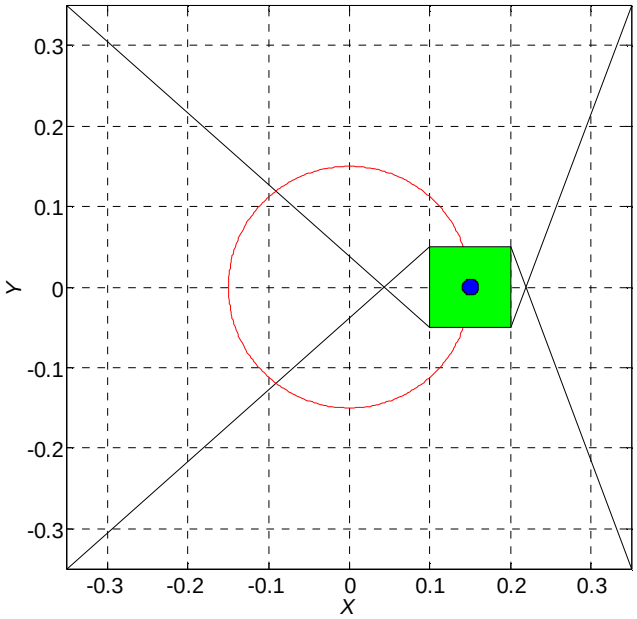

Figure 5. Planar 4-Cable Translational CDDR Example Task

In the simulated example the 4-cable CDDR is commanded to trace the given circle in 1 *sec* (zero external Cartesian wrench is specified). We define polar angle γ as the independent parameter for the circle; it is measured using the right-hand from the right horizontal to the circle radius; γ is shown at 0 (and 360°) in Fig. 5. For 'smooth' motion starting and ending at rest, we adopt trajectory generation techniques from[16]: We require that angle γ starts at zero and ends at 360° during the 1 *sec* motion; also, we require that $\dot{\gamma} = \ddot{\gamma} = 0$ at the start and end of motion, for 'smoothness'. These conditions yield a 5th order polynomial for angle γ: $\gamma(t) = 2160t^5 - 5400t^4 + 3600t^3$ (*deg*). The associated commanded (reference) Cartesian pose $\mathbf{X}_R$, velocity $\dot{\mathbf{X}}_R$, and acceleration $\ddot{\mathbf{X}}_R$ for use in the controller architecture are easy to determine. The commanded Cartesian angular values are $\phi = \dot{\phi} = \ddot{\phi} = 0$ for all motion since we are presenting a translational CDDR only.

The parameters for the dynamics equations of motion (16) for the 4-cable CDDR are (again, from our hardware design): point mass m = 0.91 *kg*; end-effector mass moment of inertia 0.00150 kgm^2; rotational shaft/pulley inertias $J_i = 0.00026$ kgm^2 (for all $i = 1, \cdots, 4$); shaft rotational viscous damping coefficients $c_i = 0.01$ *Nms* (for all $i = 1, \cdots, 4$); and $r_i = r = 3.81$ *cm* (for all $i = 1, \cdots, 4$).

The Cartesian PD controller is found by standard pole placement techniques, specifying a 0.2 *sec* settling time and 5% percent overshoot (the feedback linearization approach makes the plant appear linear, as unit inertias in the *x*, *y*, and ϕ directions; units *kg*, *kg*, and kgm^2, respectively). We design for Cartesian *x*, *y*, and ϕ directions independently, with the same settling time and percent overshoot specifications. Gain $\mathbf{K}_P$ is a 3x3 diagonal matrix with equal gains of $K_P = 839.9$ on the diagonal, and gain $\mathbf{K}_D$ is a 3x3 diagonal matrix with equal gains of $K_D = 40$ on the diagonal.

A Matlab *Simulink* simulation based on the controller architecture of Fig. 4 and the methods of this article was developed to produce the results given in this section. Two control simulations of the dynamics

model are presented in this section for the 4-cable CDDR, first without and then with the on-line minimum torque estimation algorithm of Fig. 4.

Figures 6a-c show the minimum actuator torques, simulated actuator torques, and simulated cable tensions, respectively, for the circle task, *without* the on-line minimum torque estimation algorithm.

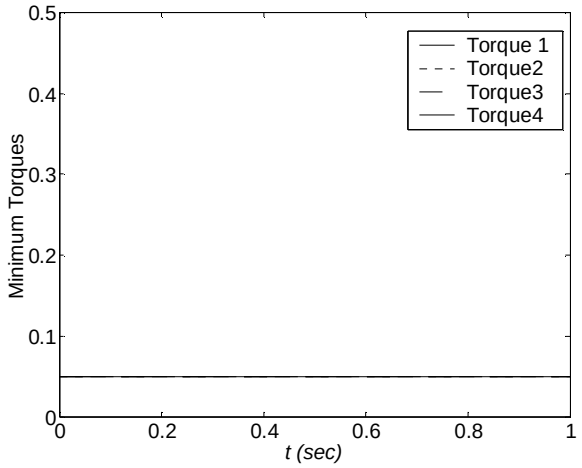

Figure 6a. Minimum Actuator Torques

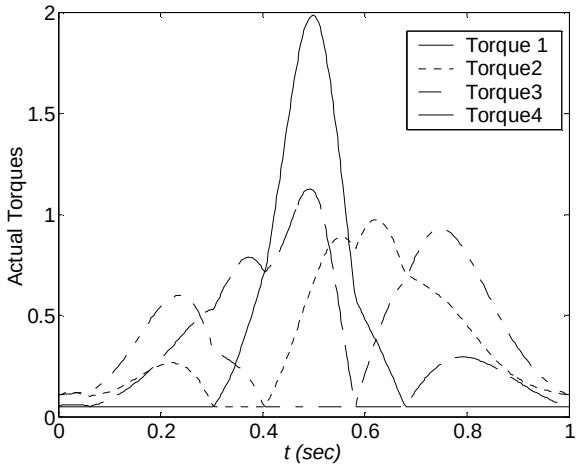

Figure 6b. Simulated Actuator Torques

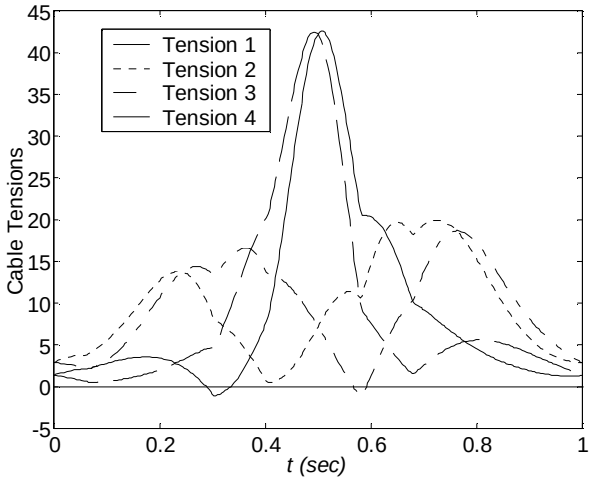

Figure 6c. Simulated Cable Tensions

As shown in Fig. 6a, for the simulation *without* the on-line minimum torque estimation algorithm, the minimum torques are constant and identical for all four actuators, taking a user-specified value of 0.05 *Nm* in this example. The control torques, calculated by the optimal method in the Virtual to Real Calculation block of Fig. 4, but without the minimum torque estimation algorithm, are shown in Fig. 6b. Actuator torques 1 and 4 peak near the center of motion time, due to the maximum velocity occurring at this point; torque 3

peaks twice, nearer the start and end of motion. During motion all four torques at different times yield negative values in the Virtual to Real Calculation, but these are limited to a small positive value, the constant specified minimum torque of 0.05 *Nm*, using the actuation redundancy. The associated simulated cable tensions resulting from the simulated motion considering the dynamics model are shown in Fig. 6c. Without considering the dynamic minimum torque estimation block of Fig. 4, cable tensions 1 and 3 become negative and thus slack at different times during the simulated motion. Clearly this is unacceptable as control would be lost in these ranges of motion and large Cartesian errors result. Thus, the constant minimum actuator torque specification is suitable only for pseudostatic motions, not for dynamic motions with high velocities and accelerations.

Figures 7a-c show the minimum actuator torques, simulated actuator torques, and simulated cable tensions, respectively, for the simulated circle task, *with* the on-line minimum torque estimation algorithm. As shown in Fig. 7a, for the simulation *with* the on-line minimum torque estimation algorithm, the minimum torques are no longer constant, but vary (greater than the minimum positive torque) so that no cable tensions will go negative in the dynamics model. The control torques, obtained by including the on-line minimum torque estimation algorithm in the Virtual to Real Calculation, are shown in Fig. 7b. Again, during motion all four torques yield negative values but these are limited to the minimum torque of 0.05 *Nm* in these ranges, using the actuation redundancy. Though Figs. 6a and 7a are quite different (minimum torques without and with the minimum torque estimation), the resulting control torques of Figs. 6b and 7b are similar, though not identical. The simulated cable tensions considering the dynamics model are shown in Fig. 7c. By including the on-line, dynamic minimum tension estimation block, each cable tension never becomes negative and thus control is maintained at all times. In Fig. 7c we allow zero cable tension as a minimum; in practice a small positive value should be used instead. Figs. 6c and 7c are very similar in shape and magnitude; however, Fig. 7c is a big improvement over Fig. 6c, where two cable tensions were negative for two portions of the motion. Thus, we must include the on-line minimum tension estimation algorithm for dynamic motions.

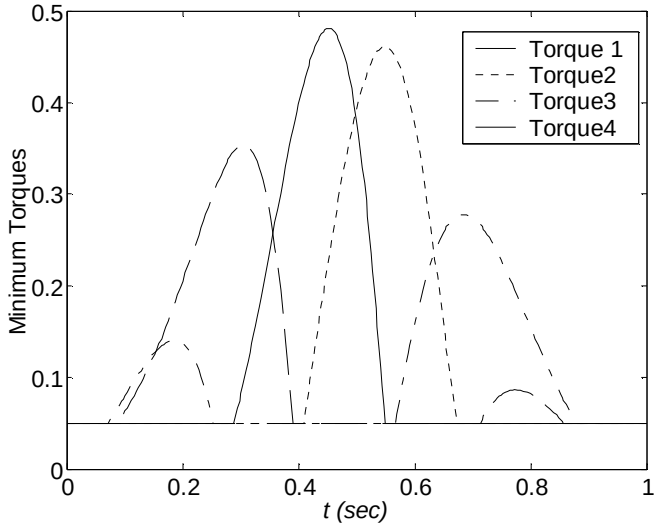

Figure 7a. Minimum Actuator Torques

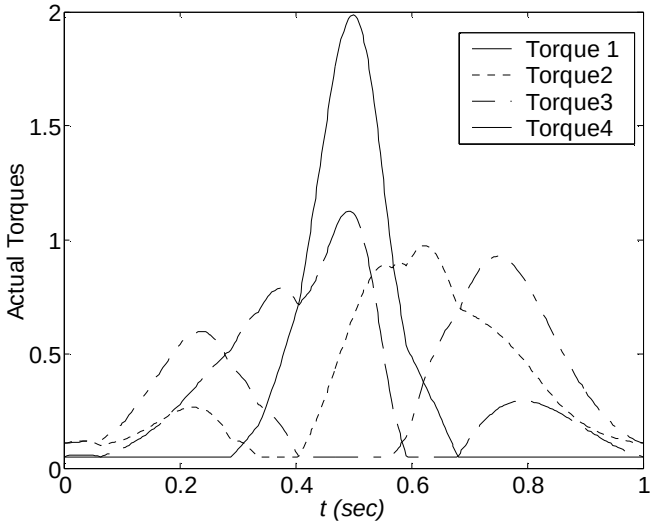

Figure 7b. Simulated Actuator Torques

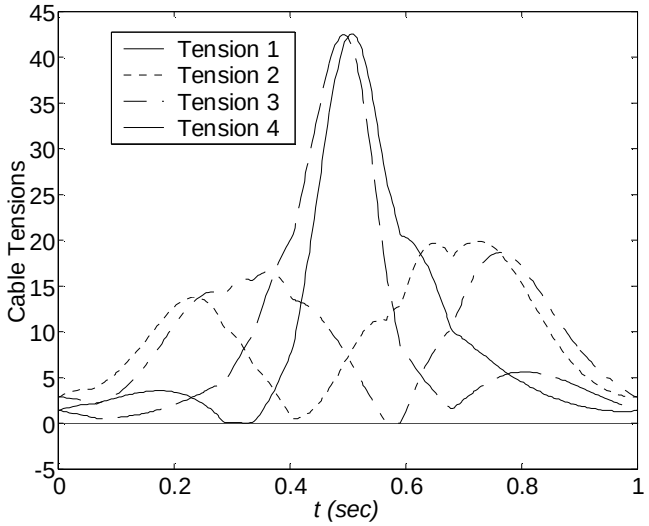

Figure 7c. Simulated Cable Tensions

For the latter example only (i.e. including the on-line minimum tension estimation algorithm), Fig. 8 shows the simulated ϕ tracking error. Since the 4-dof CDDR is used for translations only, we wish to maintain ϕ = 0 for all motion. Again, this is done to avoid the cable interference and limited statics workspace problems inherent in CDDRs with large rotational motions. In the simulation, the error remains very low, less than 4.6×10^{-6} *deg*. The error appears to be increasing with time, but with such a low magnitude, we will accept this error until we can perform experimental validation in the future.

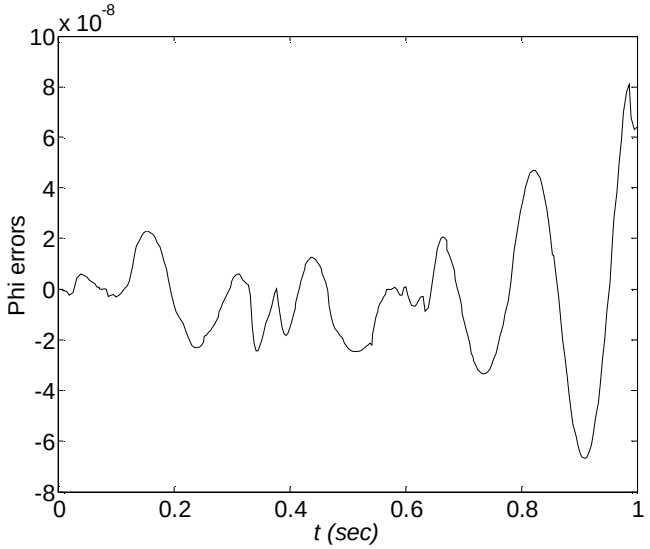

Figure 8. Simulated ϕ Tracking Error

7. CONCLUSION

This article studies a planar translational in-parallel-over-actuated cable-direct-driven robot (CDDR). The motivation behind this work is to improve the serious cable interference and negative cable tensions possible with existing CDDRs that guide both translational and rotational freedoms. Only the translational portion is considered in this article. Kinematics and statics modeling is presented, followed by a discussion of the statics workspace (the space wherein all possible Cartesian forces and moments may be exerted with only positive cable tensions). Dynamics modeling and control simulation with feedback linearization for the planar translational 4-dof CDDR with one degree of actuation redundancy were then presented. Examples were given to compare this planar CDDR in the same task, without and with an on-line dynamic minimum torque estimation algorithm.

It was found that the on-line dynamic minimum torque estimation algorithm we introduced was required for dynamic CDDR motions with high velocities and accelerations. Otherwise, the simulation revealed that some cables become slack during motion and thus control is lost. The computed-torque, or feedback linearization technique performed perfectly in simulation, i.e. when we assume we know the dynamic model perfectly, the inertial effects and nonlinear dynamics terms are cancelled perfectly. Therefore,

in the future we will focus on implementing robust control techniques to preserve good error tracking despite modeling uncertainties, using our experimental hardware.

Our future work plans also include dynamic stiffness modeling, more complete dynamics modeling (cable inertia and stiffness, plus Coulomb friction, among others), hardware implementation, and experimental validation of our results.

REFERENCES

1. J.S. Albus, R. Bostelman, and N.G. Dagalakis, 1993, "*The NIST ROBOCRANE*", Journal of Robotic Systems, 10(5): 709-724.

2. P.D. Campbell, P.L. Swaim, and C.J. Thompson, 1995, "*Charlotte Robot Technology for Space and Terrestrial Applications*", 25th International Conference on Environmental Systems, San Diego, SAE Article 951520.

3. R. Lindemann and D. Tesar, 1989, "*Construction and Demonstration of a 9-String 6-DOF Force Reflecting Joystick for Telerobotics*", NASA International Conference on Space Telerobotics, (4): 55-63.

4. S. Walairacht, Y. Koike, and M. Sato, *"A new haptic display for both-hands-operation: SPIDAR-8"*, 1999 IEEE International Symposium on Intelligent Signal Processing and Communication Systems: 569-72.

5. S. Kawamura and K. Ito, 1993, *"New Type of Master Robot for Teleoperation Using a Radial Wire Drive System"*, Proceedings of the IEEE/RSJ International Conference on Intelligent Robots and Systems, Yokohama, Japan, July 26-30, 55-60.

6. R.L. Williams II, 1998, *"Cable-Suspended Haptic Interface"*, International Journal of Virtual Reality, 3(3): 13-21.

7. R.G. Roberts, T. Graham, and T. Lippitt, 1998, "*On the Inverse Kinematics, Statics, and Fault Tolerance of Cable-Suspended Robots*", Journal of Robotic Systems, 15(10): 581-597.

8. R.L. Williams II and P. Gallina, "*Planar Cable-Direct-Driven Robots: Design for Wrench Exertion*", Journal of Intelligent and Robotic Systems, final manuscript, October 2001.

9. W. Choe, H. Kino, K. Katsuta, and S. Kawamura, 1996, *"A Design of Parallel Wire-Driven Robots for Ultrahigh Speed Motion Based on Stiffness Analysis"*, ASME Japan/USA Symposium on Flexible Automation, 1:159-166.

10. S. Kock and W. Schumacher, 2000, *"Control of Fast Parallel Robot with a redundant Chain and Gearboxes: Experimental Results"*, IEEE International Conference on Robotics and Automation: 1924-1929.

11. G. Barette and C.M. Gosselin, 2000, "*Kinematic Analysis and Design of Planar Parallel Mechanisms Actuated with Cables*", ASME Design Technical Conferences, Baltimore, MD.

12. Y. Shen, H. Osumi, and T. Arai, 1994, *"Manipulability Measures for Multi-wire Driven Parallel Mechanisms"*, IEEE International Conference on Industrial Technology, 550-554.

13. L.W. Tsai, 1999, Robot Analysis: The Mechanics of Serial and Parallel Manipulators, Wiley, New York.

14. C.M. Gosselin, 1996, "Parallel Computation Algorithms for the Kinematics and Dynamics of Planar and Spatial Parallel Manipulators", *Journal of Dynamic Systems, Measurement, and Control*, 118(1): 22-28.

15. F.L. Lewis, C.T. Abdallah, and D.M. Dawson, 1993, Control of Robot Manipulators, MacMillan, New York.

16. J.J. Craig, 1989, Introduction to Robotics: Mechanics and Control, Addison Wesley Publishing Co., Reading, MA.